

---

# Stormwater plume detection by MODIS imagery in the southern California coastal ocean

---

Nikolay P. Nezlin, Paul M. DiGiacomo<sup>1</sup>, Dario W. Diehl, Burton H. Jones<sup>2</sup>, Scott C. Johnson<sup>3</sup>, Michael J. Mengel<sup>4</sup>, Kristen M. Reife<sup>2</sup>, Jonathan A. Warrick<sup>5</sup> and Menghua Wang<sup>1</sup>

## ABSTRACT

Stormwater plumes in the southern California coastal ocean were detected by MODIS-Aqua satellite imagery and compared to ship-based data on surface salinity and fecal indicator bacterial (FIB) counts collected during the Bight'03 Regional Water Quality Program surveys conducted in February and March of 2004 and 2005. MODIS imagery was processed using a combined near-infrared/shortwave-infrared (NIR-SWIR) atmospheric correction method, which substantially improved normalized water-leaving radiation (nLw) optical spectra in coastal waters with high turbidity. Plumes were detected using a minimum-distance supervised classification method based on nLw spectra averaged within the training areas, defined as circular zones with 1.5- to 5.0-km radii around field stations with a surface salinity of  $S < 32.0$  ("plume") and  $S > 33.0$  ("ocean"). The plume optical signatures (i.e., the nLw differences between "plume" and "ocean") were most evident during the first two days after the rainstorms. To assess the accuracy of plume detection, stations were classified as "plume" and "ocean" using two criteria: 1) "plume" included the stations with salinity below a certain threshold estimated from the maximum accuracy of plume detection; and 2) FIB counts in "plume" exceeded the California State Water Board standards. The salinity threshold between "plume" and "ocean" was estimated as 32.2. The total accuracy of plume detection in terms of surface salinity was not high (68% on average), seemingly because of imperfect correlation between

plume salinity and ocean color. The accuracy of plume detection in terms of FIB exceedances was even lower (64% on average), resulting from low correlation between ocean color and bacterial contamination. Nevertheless, satellite imagery was shown to be a useful tool for estimating the extent of potentially polluted plumes; such estimates were hardly achievable by direct sampling methods, primarily because the grids of ship-based stations covered only small parts of the plumes that can be detected via synoptic MODIS imagery. In most southern California coastal areas, the zones of bacterial contamination were much smaller than the areas of turbid plumes; an exception was the plume of the Tijuana River, where the zone of bacterial contamination was comparable to the zone of plume detected by ocean color.

## INTRODUCTION

This study focuses on developing the ability to routinely detect and classify stormwater runoff plumes in the Southern California Bight (SCB) for the purpose of synoptic water quality assessments in this region. Plumes are identified as water masses with decreased salinity relative to ambient ocean water. Such gradients in salinity can only be presently measured through in situ measurements. Salinity cannot yet be measured from space (nor in the foreseeable future with necessary resolution for coastal applications), although a high correlation between salinity and "ocean color" parameters has

---

<sup>1</sup> National Atmospheric and Oceanic Administration/National Environmental Satellite, Data, and Information Service, Center for Applications and Research, Camp Springs, MD

<sup>2</sup> University of Southern California, Department of Biological Sciences, Los Angeles, CA

<sup>3</sup> Aquatic Bioassay and Consulting Laboratories, Ventura, CA

<sup>4</sup> Orange County Sanitation District, Fountain Valley, CA

<sup>5</sup> United States Geological Survey, Coastal and Marine Geology Program, Santa Cruz, CA

been shown in many coastal regions (Monahan and Pybus 1978, Vasilkov *et al.* 1999, Siddorn *et al.* 2001, Miller and McKee 2004). The color of plumes results from high concentrations of suspended sediments and Colored Dissolved Organic Matter (CDOM). Suspended sediments increase backscattering in the longer wavelength portion of the visible spectrum (Toole and Siegel 2001, Miller *et al.* 2005); CDOM absorbs light at short wavelengths (Del Castillo 2005) and CDOM concentration is more conservative than suspended sediments. Emerging plumes contain high concentrations of suspended sediments, which rapidly decrease with time due to gravitational sedimentation (Warrick *et al.* 2004b, Ahn *et al.* 2005). Decreases in CDOM occur due to photodegradation, but this process takes weeks to months (Vodacek *et al.* 1997, Opsahl and Benner 1998).

Ocean color satellite imagery could be used to estimate when and where high concentrations of contaminants occur, because concentrations of contaminants in stormwater plumes (e.g., fecal indicator bacteria) are related to salinity (Bay *et al.* 2003, Nezlin *et al.* 2007), which, in turn, can be related to ocean color. In turn, this information could be especially useful to coastal managers and governing agencies who are required to perform additional monitoring and close beaches when contaminants exceed various standards (State Water Resources Control Board 2005).

Previous studies of stormwater plumes based on ocean color satellite imagery were focused on physical forcing regulating plume dynamics (e.g., Estournel *et al.* 1997, Froidefond *et al.* 1998, Siegel *et al.* 1999, Warrick and Fong 2004, Warrick *et al.* 2007) and/or estimation of the amount of discharged sediments (e.g., Lira *et al.* 1997, Ouillon *et al.* 1997, Warrick *et al.* 2004b,c). In southern California, previous studies (e.g., the "Plumes and Blooms" program) studied spatial and temporal characteristics of the plumes of discharged sediment and associated with them phytoplankton blooms in the Santa Barbara Channel (Toole and Siegel 2001, Otero and Siegel 2004). Our previous satellite-based plume studies (e.g., Nezlin and DiGiacomo 2005, Nezlin *et al.* 2005) focused primarily on multi-year analysis of plume dynamics, whereas the present effort is geared toward developing an event detection, classification, and impact assessment system for near real-time satellite-based synoptic characterizations of water quality. The results of this study could be used to develop a cost effective water quality monitoring

strategy in the SCB and other urban coastal regions. This type of strategy would provide environmental managers with information on coastal water quality that is both faster and spatially more extensive than the exclusively in situ, shipboard sampling techniques currently in use. However, such satellite-based information would merely complement, and not eliminate, field based sampling efforts.

In analyzing the accuracy of plume detection, the accuracy statistics for "plume" (i.e., potentially polluted waters) and "ocean" (i.e., potentially clean waters) were assessed separately, with commission and omission errors recorded for each classification (Congalton and Green 1999, Lillesand and Kiefer 2000). Commission error is the chance to erroneously assign pixels to a particular class; omission error is the chance to lose pixels by erroneously excluding them from that class. Commission error for "plume" and omission error for "ocean" indicate the chance to erroneously detect a plume (and, potentially by extension, recommend a beach closure) in the absence of contamination. The consequences of this kind of inaccuracy can be economic loss for the recreation industry. In contrast, omission error for "plume" and commission error for "ocean" indicate the chance to miss contaminated plume waters, resulting in potential health risks for beach visitors.

For this study, the satellite images collected by the Moderate Resolution Imaging Spectroradiometer (MODIS) on the Aqua satellite platform during the Bight'03 Regional Water Quality Program surveys in February to March of 2004 and 2005 were processed using the combined NIR-SWIR method of atmospheric correction (Wang and Shi 2007), which was developed especially for analysis of coastal data. Optical signatures (i.e., the spectra of nLw in the plume core (surface salinity  $S < 32.0$ ), plume edge ( $32.0 \leq S \leq 33.0$ ), and ocean ( $S > 33.0$ ) waters were compared. Then, the averaged optical signatures of the plume core and ocean were used as endmembers (training areas) to classify all pixels from the MODIS-Aqua imagery into two classes: "plume" and "ocean". To estimate the accuracy of classification, the entire range of S measurements, including plume core, plume edge, and ocean, was used. Also, California State Water Board FIB exceedance standards were used as another measure of plume detection accuracy. Finally, plume area size was assessed, and plumes detected using remotely-sensed ocean color were compared with the plumes detected on the basis of decreased salinity and bacterial contamination.

## METHODS

### Study Site

Stormwater plumes are a main source of pollution in the southern California (SC) coastal ocean. Noble *et al.* (2003) found that 96% of the shoreline met water quality standards during dry weather, but 58% of the shoreline failed to meet water quality standards during wet weather. The rainy season in SC occurs from late fall to early spring (Dailey *et al.* 1993) and consists of episodic storm events, which contribute more than 95% of the total annual runoff to the SCB (Schiff *et al.* 2000). SC is a highly developed urban area where increased impervious surface area leads to greater runoff and contaminant loading to the ocean, producing up to 90% more runoff than unaltered watersheds (Miller *et al.* 2002). Rapid surface flow following rainstorms results in plumes emerging and increasing to a maximum size during a short period (one to two days) after these storms (Nezlin *et al.* 2005).

To a large extent, the optical signatures of plumes in SC result from high concentrations of suspended sediments and CDOM discharged with stormwater (Mertes and Warrick 2001, Warrick and Milliman 2003, Warrick *et al.* 2004a). Resuspension of sediments from the ocean bottom does not play a significant role in the SCB, because the continental shelf is narrow. Washburn *et al.* (1992) studied resuspension in the western part of the San Pedro Shelf and only observed high concentrations of sediments resuspended by water circulation within 15 m of the bottom. Throughout the SCB, the ocean bottom exceeds 15 m within 1 km offshore; as such, the sediments resuspended from the bottom by winds, waves, and currents are not likely to be a significant factor for purposes of this analysis.

The propagation, direction, and persistence of stormwater plumes in the SCB are variable depending on locally and remotely modulated circulation patterns (Nezlin and DiGiacomo 2005). Alongshore movement of stormwater plumes in the SCB prevails over acrossshore movement (Warrick *et al.* 2007). Downcoast propagation of plumes is typical of the spring period and results from wind driven upwelling-favorable coastal circulation associated with a spring transition (Strub *et al.* 1987, Strub and James 1988, Lynn *et al.* 2003).

### Data Collection and Analysis

Ship-based data and MODIS imagery were col-

lected during the Bight'03 Regional Water Quality Program surveys conducted in February and March of 2004 and 2005 (Warrick *et al.* 2007). Due to the inconsistent nature of rainfall within SC, sampling was carried out in two sub-regions, north/central and south (San Diego), independent of each other. Sampling event #1 was initiated by the storms February 22-23, 2004, in the San Diego area and three days later, on February 25-26, in the northern and central areas. Sampling event #2 was initiated February 11-12, 2005, in the San Diego area and almost six weeks later, on March 23, 2005, in the northern and central areas. Analysis included observations collected over eight days (February 24, 27, 28, and 29; March 1, 2004 and February 13, March 23 and 25, 2005) when both satellite images and ship-based sampling were available.

The satellite data used in this study were collected by the NASA MODIS sensor operating onboard the near-polar sun-synchronous satellite platform Aqua orbiting at 705 km altitude (Esaías *et al.* 1998). Aqua passes the equator south to north at ~13:30 local time; as such, all the images were acquired within two hours after local noon (20:00 to 22:00 UTC). The MODIS sensor collects data in 36 spectral bands, from 400 to 14,000 nm; of which only some are useful for ocean applications. The radiances measured by the satellite sensors were converted into nLw. The nLw parameter is defined to be the upwelling radiance just above the sea surface, in the absence of an atmosphere, and with the sun directly overhead (Gordon and Wang 1994).

In this study, MODIS imagery was processed using a combined NIR-SWIR atmospheric correction approach (Wang and Shi 2007). The traditional method of atmospheric correction used for processing of Sea-viewing Wide-Field-of-view Sensor (SeaWiFS) and MODIS imagery is based on two NIR bands used for identifying aerosol type and correcting aerosol contributions at the visible wavelengths (Gordon and Wang 1994, Gordon 1997). For MODIS, two NIR bands centered at 748 and 869 nm are used, and the ocean is assumed to be black at these two wavelengths. This assumption works well for open ocean waters. In turbid coastal waters, however, ocean contribution to NIR is significant, resulting in substantial errors in derived ocean color products (Wang and Shi 2005). In this case, two SWIR bands (e.g., 1240 and 2130 nm) are preferable for atmospheric correction because ocean surface reflectance in SWIR is close to zero regardless of

suspended matter and CDOM concentrations (Wang 2007, Wang *et al.* 2007). However, the MODIS SWIR were designed for land and atmosphere applications with substantially lower sensor band signal-to-noise ratio (SNR) values. For accurate ocean color products, much better sensor SNR values for the SWIR bands are required (Wang 2007). Thus, a combined NIR-SWIR method (Shi and Wang 2007, Wang and Shi 2007) was used in this study for the MODIS ocean color data processing.

In the combined NIR-SWIR method of atmospheric correction, a turbidity index (Shi and Wang 2007) based on MODIS-measured radiances at the NIR and SWIR bands is computed to discriminate between turbid coastal and non-turbid ocean waters. For the pixels identified as turbid waters, the SWIR method of atmospheric correction is applied; for non-turbid waters, the NIR method is used (see details in Wang and Shi 2007). Previous studies illustrated that this approach results in good quality ocean color products without obvious discontinuities (Wang and Shi 2007).

For this study, nLw radiances were estimated at eight MODIS ocean visible NIR wavelengths: 412, 443, 488, 531, 551, 667, 678, and 748 nm. MODIS pixel size is ~1 km. The pixels associated with atmospheric correction failure, land, cloud or ice, stray light, and sun glint were excluded from analysis. In addition, pixels with L2 flags for “shallow water”, “aerosol iterations exceeded maximum”, “atmospheric correction is suspect”, and “high degree of polarization” were masked.

Ship-based samples were collected in four geographic regions that represent the river mouths of the largest southern California watersheds (Figure 1). These regions included (from the north): the eastern Santa Barbara Channel (Santa Clara and Ventura Rivers); Santa Monica Bay (Ballona Creek); the San Pedro Shelf (Los Angeles, San Gabriel and Santa Ana Rivers and Newport Bay); and the southern Bight (San Diego and Tijuana Rivers). Sampling occurred on regularly spaced grids for each region. The primary intent of the grids was to sample the nearshore discharge areas and assess water quality there, not necessarily to track plumes as they advected away from the river mouth regions. The primary method of investigation was shipboard profiling of the plumes with an enhanced CTD system: conductivity, temperature, depth, dissolved oxygen, pH, transmissometer, chlorophyll fluorometer, and CDOM fluorometer data (CTD+). Water samples

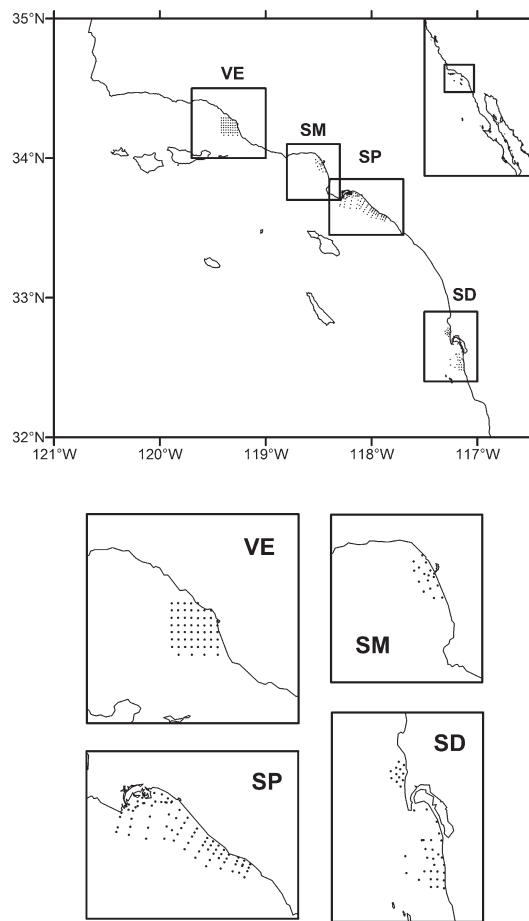


**Figure 1. Stations for ship-based sampling during the Bight'03 Program in four regions in the Southern California Bight: Ventura (VE); Santa Monica Bay (SM); San Pedro Shelf (SP); San Diego (SD).**

were taken at a depth of 1 m for most sites and at subsurface depths below the buoyant plume for a limited number of sites. Samples were analyzed for total suspended solids, chlorophyll, macronutrients (Si, N, P), FIB (total coliforms, fecal coliforms, and *Enterococcus* sp.) and toxicity. Surface salinity (derived from CTD+ conductivity) and FIB were a focus of this study. The stations were classified as exceeding California State Water Board standards when the FIB counts in single sample were >10,000 for total coliforms; >400 for fecal coliforms; and >104 for *Enterococcus* sp. (State Water Resources Control Board 2005).

All ship-based stations were classified into plume core ( $S < 32.0$ ), plume edge ( $32.0 \leq S \leq 33.0$ ) and ocean ( $S > 33.0$ ) assuming normal ocean salinity in the SCB as 33.4 - 33.6 (Hickey 1993). Optical spectra (nLw) were selected from MODIS images collected during the same day as ship-based sampling from circles with 1.5-km radii centered on the

location of each ship-based station. Masked pixels from MODIS imagery were excluded from statistical computations. For each nLw (412 - 748 nm), median and quartile (25% and 75%) statistics were calculated for each class. Optical spectra (nLw medians) of plume cores ( $S < 32.0$ ) and ocean ( $S > 33.0$ ) were used as endmembers (training areas) for supervised classification.

A minimum distance supervised classification technique (Richards 1999) used the mean vectors of each endmember (i.e., eight-nLw vectors of plume and ocean water, respectively) and calculated the Euclidean distance from each image pixel to the mean vector for each class. Each pixel from the MODIS image was classified to the nearest class (i.e., “plume” or “ocean”). The accuracy of classification was assessed by comparing the MODIS imagery pixels selected from the circles of variable size (radius (R) = 1.5 - 5.0 km) centered on the location of each ship-based station; the classes (“plume” or “ocean”) to which these stations were attributed were based on surface salinity or FIB exceedances. Varied circle sizes were used for two reasons: first, satellite navigation may not be accurate to a pixel (see Bailey and Werdell 2006) and the level of this kind of spatial inaccuracy is uncertain; second, it is important to take into account the time lag between ship-based data collection (surveys were typically conducted from 7 a.m. to 4 p.m. local time) and MODIS-Aqua imagery (taken about 1 to 2 p.m.). A horizontal velocity of 50 cm/second (equal to ~1.8 km/hour) such as that observed in southern California river plumes (Warrick *et al.* 2007) can move the plume boundary as far as 5 to 10 km during a few hours, which can dramatically increase spatial inaccuracy between water surface parcels measured by satellites and those obtained by research vessels. Consequently, the present study also varied R values when selecting the pixels from the classified MODIS imagery to determine which R value corresponded to maximum classification accuracy (see Results).

To assess the accuracy of classification in terms of salinity, the present study used a larger set of salinity data than the data set used for endmember estimation. In addition to “plume core” and “ocean”, the larger data set included stations attributed to “plume edge” ( $32.0 \leq S \leq 33.0$ ). Varied S thresholds between “plume” and “ocean” were used, and the S value resulting in maximum total accuracy were selected.

As accuracy measures, total accuracy, commis-

sion and omission errors for “plume” and “ocean” classes, and KHAT statistic (Congalton and Green 1999, Lillesand and Kiefer 2000) were used. Total accuracy is the percentage of correctly classified pixels. KHAT is a statistical measure of the difference between actual total classification accuracy and erroneous accuracy measure that can be obtained by completely random assignment of pixels to classes. The commission error for “plume” and the omission error for “ocean” both illustrate the number of pixels erroneously classified as “plume” instead of “ocean” (N-lost). However, these statistics are not equivalent because the “plume” commission error is N-lost divided by the total number of pixels in the “plume” class, while the “ocean” omission error is N-lost divided by the total number of pixels in the “ocean” class.

## RESULTS

### Optical Spectra of Stormwater Plumes

The optical signatures of the plume core, plume edge, and ocean were significantly different from one another (Figure 2; Table 1); these differences can be explained by backscattering of suspended sediments and absorption of CDOM. At longer wavelengths (488 - 748 nm), nLw in the plume core exceeded nLw in ocean waters; this difference appeared to be a result of backscattering of suspended sediments. At 412 nm, nLw in plumes was lower when compared with ocean waters, which could potentially be explained by CDOM absorption. In plume edge waters, the shape of nLw spectrum was similar to the plume core, but nLw was lower at all wavelengths, excluding the shortest 412 nm (Figure 2; Table 1). This suggests that although diminished in concentration within the plume edge, the optical components affecting remotely-sensed reflectance are the same as those in the plume core.

The optical signatures of the plumes changed with time (Figure 2; Table 1). During the first two days after storm events, the difference between the plume core and the ocean was similar to the pattern revealed on the basis of all observations. However, the optical spectrum of the plume edge was much closer to the plume core during the first two days after the storm than during the third and fourth days after the storm; this can be explained by the presence of high sediment and CDOM concentrations in the plume (including both core and edge) during a short period after the plume emergence. During the following three to four days, the optical spectrum of the

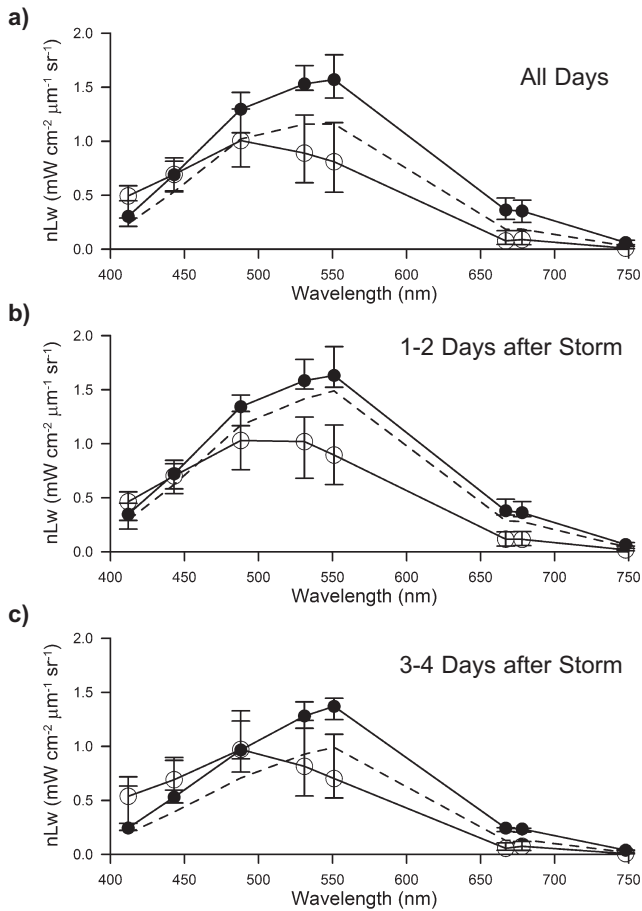


**Figure 2. Normalized water-leaving radiation (nLw) spectra of the plume core ( $S < 32.0$ ; black circles), plume edge ( $32.0 \leq S \leq 33.0$ ; dashed line), and ocean waters ( $S > 33.0$ ; open circles) averaged over all observations (a), first-second (b), and third-fourth (c) days after rainstorm.**

ocean remained unchanged, but the spectra of the plume edge and the plume core changed. Within the plume, all nLw decreased consistent with decreases in suspended sediment concentration and mixing. CDOM concentration within the plume remained high, and the relative contribution of the CDOM signal into the plume optical signature at short wavelengths (412 and 443 nm) increased. At the plume edge, nLw at wavelengths  $> 488$  nm were lower than those in the plume core as would be expected with lower concentration of suspended sediments.

### Accuracy of Plume Detection

The best accuracy of classification was achieved when the S threshold between “plume” and “ocean” was 32.2. Various S thresholds were tested within the range 32.0 - 33.0 and various R were tested within the range 1.5 - 5.0 km (R = the radius of a circular area centered at ship-based station coordinates within which image pixels were selected for assessment accuracy). At  $S = 32.2$ , the total accuracy of classification reached its maximum (67 - 70%) and was almost independent of R. Other statistics, however, indicated that best accuracy was at  $R = 1.5$  km. KHAT, the statistical significance of total accuracy at the given number of classes and measurements, decreased from 31% at  $R = 1.5$  km to 24% at  $R = 5.0$  km (Figure 3a). Plume omission error was larger than other statistics dependent on R, increasing from 14% at  $R = 1.5$  km to 33% at  $R = 5.0$  km. The latter statistic is especially important in water quality analysis because it illustrates the chance to

**Table 1. The sign and significance of differences (p) based on Mann-Whitney U-test between nLw in the plume core (PC;  $S < 32.0$ ), ocean (OC;  $S > 33.0$ ), and plume edge (PE;  $32.0 \leq S \leq 33.0$ ) for all observations, the first two days after a rainstorm, and the third to fourth days after a rainstorm (values are presented in Figure 2). Number of stations in PC, OC, and PE, respectively: total = 22, 64, and 89; the first two days after a rainstorm = 18, 31, and 55; third to fourth days after rainstorms = 4, 33, and 34. (+/-) indicates that nLw in the first class (PC or PE) was significantly higher/lower than nLw in the second class; (=) indicates that the differences were insignificant ( $p > 0.05$ ).**

nLw (nm)	All Days			1 - 2 Days after Rainstorm			3 - 4 Days after Rainstorm		
	PC>OC	PC>PE	PE>OC	PC>OC	PC>PE	PE>OC	PC>OC	PC>PE	PE>OC
412	(-) 0.007	(=) 0.218	(-) 0.000	(=) 0.078	(=) 0.578	(-) 0.000	(=) 0.195	(=) 0.134	(-) 0.000
443	(=) 0.984	(+) 0.024	(-) 0.004	(=) 0.561	(=) 0.101	(=) 0.276	(=) 0.525	(=) 0.083	(-) 0.005
488	(+) 0.004	(+) 0.003	(=) 0.959	(+) 0.004	(+) 0.023	(=) 0.161	(=) 0.769	(=) 0.083	(=) 0.087
531	(+) 0.000	(+) 0.001	(+) 0.000	(+) 0.000	(+) 0.020	(+) 0.001	(=) 0.078	(=) 0.064	(=) 0.142
551	(+) 0.000	(+) 0.001	(+) 0.000	(+) 0.000	(+) 0.023	(+) 0.000	(+) 0.031	(+) 0.036	(+) 0.010
667	(+) 0.000	(+) 0.000	(+) 0.000	(+) 0.000	(+) 0.007	(+) 0.000	(+) 0.013	(+) 0.024	(+) 0.000
678	(+) 0.000	(+) 0.000	(+) 0.000	(+) 0.000	(+) 0.007	(+) 0.000	(+) 0.015	(+) 0.025	(+) 0.000
748	(+) 0.000	(+) 0.000	(+) 0.000	(+) 0.000	(+) 0.009	(+) 0.000	(+) 0.011	(+) 0.017	(+) 0.000

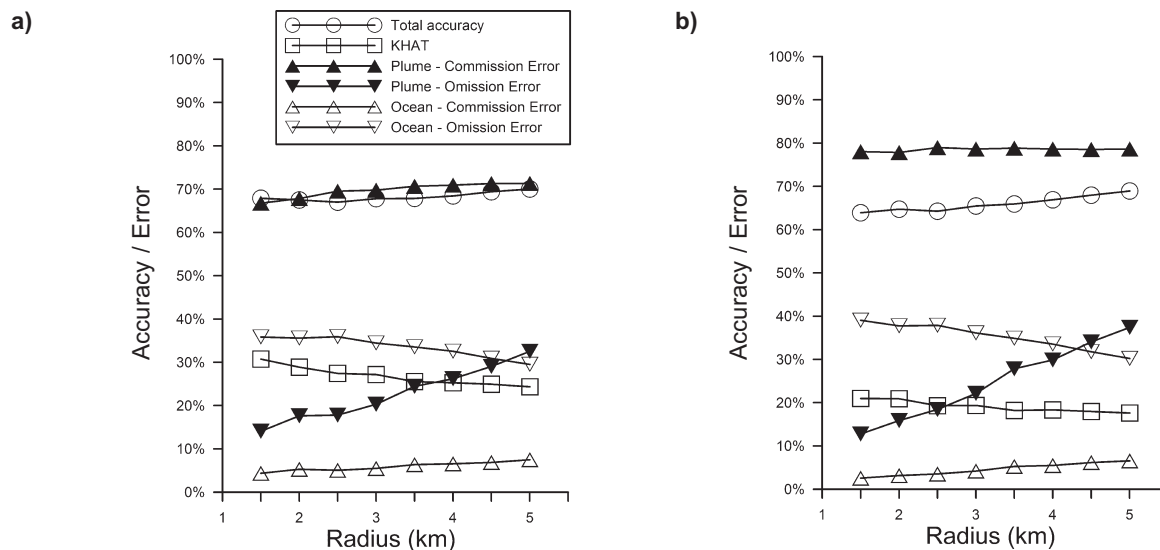


**Figure 3. Accuracy statistics (total, KHAT, and commission and omission errors for “plume” and “ocean”) of plume detection based on salinity (the threshold between “plume” and “ocean”  $S = 32.2$ ; a) and FIB counts (the threshold between “plume” and “ocean” is California State Water Board Standards exceedance; b) depending on the radius of the circle around each station where the classified pixels were selected.**

miss a polluted plume that could result in human health risk.

The accuracy of plume detection in terms of FIB exceedances was lower than in terms of salinity (Figure 3b). The total accuracy was 64 - 68%; KHAT decreased from 21% at  $R = 1.5$  km to 18% at  $R = 5.0$  km. Plume omission error was low (13%) at  $R = 1.5$  km and increased to 37% at  $R = 5.0$  km. As such, it was concluded that minimum  $R$  (i.e., 1.5 km) is the best for accuracy analysis.

Combining both salinity and FIB data in plume detection somewhat improved the accuracy statistics. When plumes were designated as the stations where either salinity was less than 32.2 or FIB counts exceeded standards, both total accuracy and KHAT slightly increased (71% and 38%, respectively).

### Stormwater Plumes in SCB

The results of the classification showed robust plume patterns located along the coast and associated with river mouths (Figures 4 - 6). The plume areas obtained from the satellite imagery significantly exceeded the areas covered by the ship-based surveys, for which station grids were not intended to capture the entire regional plumes given the time, expense, and difficulty involved in such an effort. In the Ventura region, the sampled area was restricted to the zone near the mouths of the Santa Clara

and Ventura Rivers, while the signature of the turbid plume extended downcoast, especially in March 2005 (Figure 4). Plume signatures from local discharges into Santa Monica Bay were small; however, in March 2005, the tip of a large plume from the Ventura and Santa Clara rivers was transported to the western part of Santa Monica Bay. On the San Pedro Shelf in February 2004, the plume also propagated downcoast beyond the area of the ship-based surveys (Figure 5). In spring 2005, the plume signature was not observed after the March 23 rainstorm due to cloud cover; two days later (March 25), the plume was very small. For February 28-29, 2004, and February 13, 2005, a small plume was observed in the mouth of the San Diego River (Figure 6). In the February 24, 2004 image, the Tijuana River plume was much larger than the San Diego River plume, and it propagated upcoast; in other images, its direction was southward.

Plumes frequently extended upward of 10 km offshore (e.g., Figure 4). Overall, the largest plume area size (692 km<sup>2</sup>) was observed in the Ventura region on February 28, 2004 (Table 2). During other days when the sky was clear and a significant part of the Ventura region was observed by satellite, the plumes there were also large (409 - 669 km<sup>2</sup>). Plumes of comparable size were observed on the San Pedro Shelf in February 2004 one to two days after the

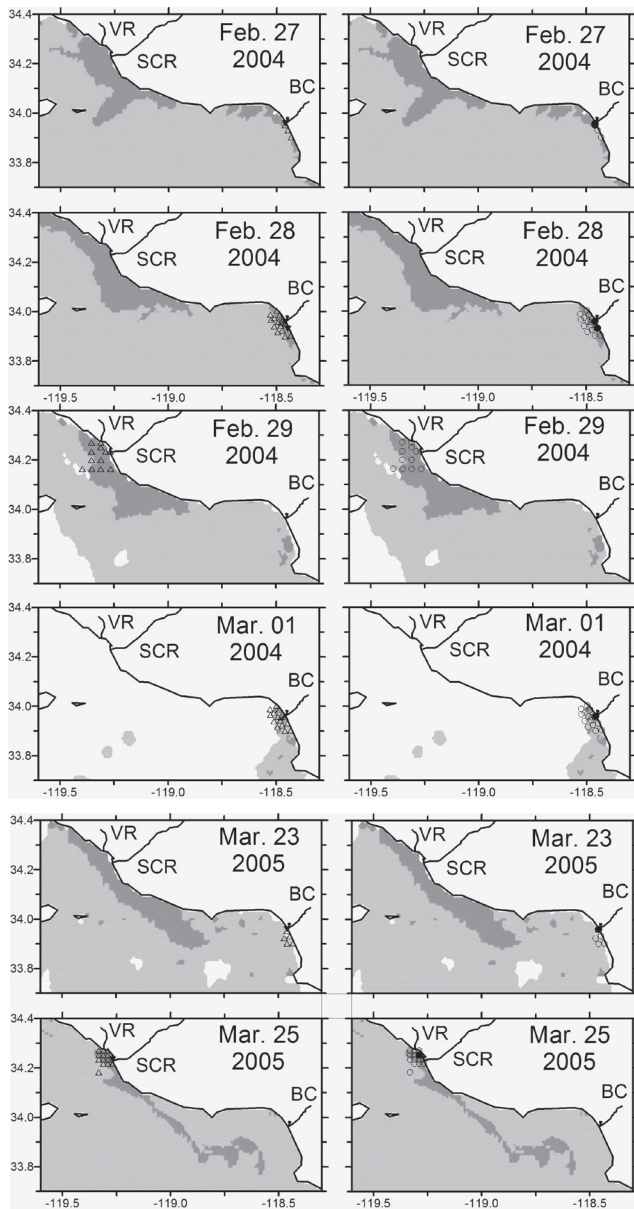


**Figure 4. Plume areas (dark shaded) in the Ventura and Santa Monica Bay regions resulting from classification of the MODIS imagery and the Bight'03 ship-based measurements of salinity and FIB counts. Light shading indicates ocean waters; white indicates the absence of MODIS imagery due to cloud cover. Black/white triangles (left) indicate bacterial counts exceeding/not exceeding California standards; black/white circles (right) indicate salinity exceeding/not exceeding 32.2. Ventura River (VR); Santa Clara River (SCR); Ballona Creek (BC).**

storm (335 - 503 km<sup>2</sup>); however, on the following day, the plume size substantially decreased (115 km<sup>2</sup>).

Maximum size of the plumes in the Ventura and San Diego regions was observed on February 28,

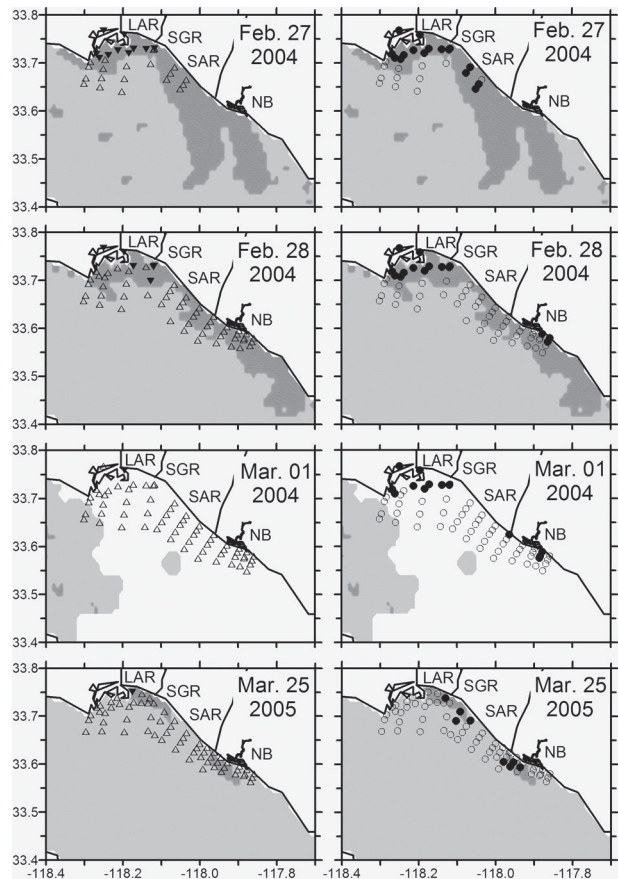


**Figure 5. Plumes on the San Pedro Shelf resulting from classification of the MODIS imagery and the Bight'03 ship-based measurements of salinity and FIB counts. For shadings and symbols (see Figure 4). Los Angeles River (LAR); San Gabriel River (SGR); Santa Ana River (SAR); Newport Bay (NB).**

2004, two days after a rainstorm (Table 2). In contrast, on the San Pedro Shelf, the maximum size of the combined plume of the Los Angeles, San Gabriel, and Santa Ana Rivers was observed one day earlier, February 27, 2004. The higher speed of plume formation on the San Pedro Shelf resulted from more intensive runoff over impervious surfaces, as the watersheds adjacent to the San Pedro Shelf region are more developed (urbanized) in comparison with more natural watersheds in the Ventura and San Diego regions.

The plume areas that were estimated using ocean surface color were significantly larger than the areas of impact calculated based on FIB exceedances interpolated over the in situ sampling grid (Table 3). No impact in terms of bacterial contamination was estimated for the Ventura and Santa Monica Bay regions. For the San Pedro Shelf, the largest area of

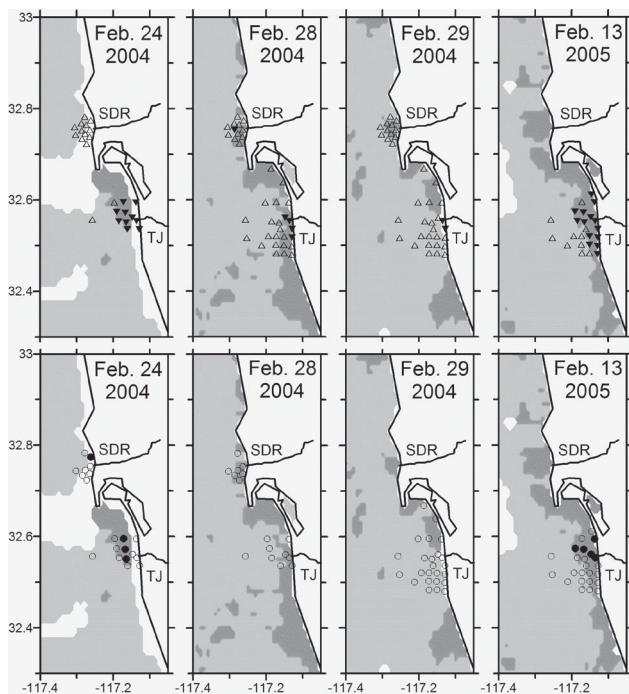


**Figure 6. Plumes in the San Diego region resulting from classification of the MODIS imagery and the Bight'03 ship-based measurements of salinity and FIB counts. For shadings and symbols (see Figure 4). San Diego River (SDR); Tijuana River (TJ).**

FIB impact was <40 km<sup>2</sup> (on the first day after the storm), which was ~6% of the plume area estimated using ocean color. In the San Diego area, the area of impact for the Tijuana River region was ~50 km<sup>2</sup> in 2004 and 50 to 100 km<sup>2</sup> in 2005 (*cf.* Figure 6). Estimated using ocean color, the Tijuana River plume was 87 to 324 km<sup>2</sup> (Table 2); the area of FIB impact was comparable to satellite observations of the plume.

## DISCUSSION

This study shows that the data collected by “ocean color” satellites (e.g., MODIS-Aqua) are a useful tool for detecting stormwater plumes and that the methods used in this study, including NIR-SWIR atmospheric correction and statistical methods of accuracy assessment, can be used in other coastal regions.

MODIS imagery can be used for the estimation of plume size and direction even in areas like the SCB where plume size is much smaller than the plumes associated with large rivers like the Mississippi (Walker 1996, DelCastillo *et al.* 2001, D'Sa and Miller 2003), the Amazon (Curtin and Legeckis 1986, Mertes *et al.* 1993, Del Vecchio and Subramaniam 2004), the Orinoco (Muller-Karger *et al.* 1989), and the Columbia (Fiedler and Laurs 1990). Ship-based data alone are inadequate to resolve plume boundaries or to provide a synoptic

**Table 2. Plume areas (km<sup>2</sup>) estimated from MODIS-Aqua imagery classified on the basis of Bight'03 ship-based sampling. Regions indicate river outfalls: Santa Clara River (SCR); Ventura River (VR); Ballona Creek (BC); Los Angeles River (LAR); San Gabriel River (SGR); Santa Ana River (SAR); Newport Bay (NB); San Diego River (SDR); Tijuana River (TJR).**

Date	Day(s) after Storm	Regions				
		Ventura (SCR + VR)	Santa Monica Bay (BC)	San Pedro (LAR+SGR+SAR+NB)	San Diego (SDR)	San Diego (TJR)
Feb.-24-2004	1 <sup>a</sup>	-	-	-	0	87
Feb.-27-2004	1	578	117	503	0	130
Feb.-28-2004	2	692	53	335	19	324
Feb.-29-2004	3	603	51	115	15	124
Mar.-01-2004	4	-	34	-	-	-
Feb.-13-2005	1 <sup>a</sup>	-	-	-	54	240
Mar.-23-2005	1	669	0.4	-	-	-
Mar.-25-2005	3	409	4	54	0	43

<sup>a</sup> Storm occurred in San Diego only

**Table 3. The size of the areas of impact (A; km<sup>2</sup>) and the size of total area sampled (T; km<sup>2</sup>). Regions indicate river outfalls (see Table 2). The survey dates in the Ventura, Santa Monica, and San Pedro regions were different than survey dates for the San Diego region. The impact areas were significantly smaller than the plume areas shown in Table 2.**

Storm	Day(s) after Storm	FIB	Survey Date	Regions						Survey Date	Region	
				Ventura (SCR + VR)		Santa Monica Bay (BC)		San Pedro (LAR+SGR+SAR+NB)			San Diego (SDR+TJR)	
				A	T	A	T	A	T		A	T
2004	1	Total coliforms		0	94	-	-	7.8	131		20.3	50
		Fecal coliforms	Feb.27	0	94	-	-	0	131	Feb.24	26.8	50
		<i>Enterococcus</i>		0	94	-	-	39.4	131		48.7	50
	2	Total coliforms		-	-	0	48	22.3	272		3.0	84
		Fecal coliforms	Feb.28	-	-	0	48	0	272	Feb.28	4.7	84
		<i>Enterococcus</i>		-	-	0	48	15.2	272		0.0	84
	3	Total coliforms		-	-	-	-	-	-		8.5	172
		Fecal coliforms	Feb.29	-	-	-	-	-	-	Feb.29	3.8	172
		<i>Enterococcus</i>		-	-	-	-	-	-		0.0	172
	4	Total coliforms		-	-	0	48	0	272		-	-
		Fecal coliforms	Mar.1	-	-	0	48	0	272		-	-
		<i>Enterococcus</i>		-	-	0	48	5.7	272		-	-
2005	1	Total coliforms		-	-	1.53	24	0	62		51.9	53
		Fecal coliforms	Mar.23	-	-	0.05	24	0	62	Feb.13	51.9	53
		<i>Enterococcus</i>		-	-	0	24	5	62		51.9	53
	2	Total coliforms		0	24	0.02	48	2.1	33		50.3	53
		Fecal coliforms	Mar.24	0	24	0	48	0	33	Feb.14	42.9	53
		<i>Enterococcus</i>		0	24	0	48	0	33		51.9	53
	3	Total coliforms		0	24	-	-	0	253		103.0	126
		Fecal coliforms	Mar.25	0	24	-	-	0	146	Feb.15	63.0	126
		<i>Enterococcus</i>		0	24	-	-	4.4	253		70.5	126
	4	Total coliforms		0	24	0	48	-	-		-	-
		Fecal coliforms	Mar.26	0	24	0	48	-	-		-	-
		<i>Enterococcus</i>		0	24	0	48	-	-		-	-

view of the direction of propagation and offshore/alongshore extension of a plume. In all of the SCB regions, the areas covered by Bight'03 ship-based sampling were smaller than the areas of stormwater plumes detected by satellite sensors (*c.f.* Warrick *et al.* 2007). This difference was largely by design given the expense and logistical difficulties of sampling such large regions. It was especially evident in the Ventura region where plumes are typically larger than those in the rest of the SCB (Nezlin *et al.* 2005). This can be explained by the large watershed area, high discharge volumes, the high concentration of discharged sediments (Otero and Siegel 2004, Warrick *et al.* 2004a), and the dynamic circulation patterns associated with the Ventura region (Harms and Winant 1998, Bray *et al.* 1999).

The general plume characteristics revealed from SeaWiFS observations in 1997 to 2003 (Nezlin and DiGiacomo 2005, Nezlin *et al.* 2005) are in accordance with the results of this study: the largest plumes were observed in the Ventura region and the smallest in the Santa Monica Bay. Maximum plume size occurred one day after a rainstorm over the San Pedro Shelf and two days after storms in other regions. The differences among SCB watersheds are illustrated by the comparison between the ocean color imagery and the areas of FIB impact. In particular, a large natural watershed of the Ventura and Santa Clara Rivers releases its water and FIB loads more slowly into the coastal waters, while a more urbanized large watershed off the Los Angeles and San Gabriel Rivers releases FIB loads much more quickly due to channelized flow. Another factor reg-

ulating FIB impact in the San Pedro region is that the Los Angeles River and two major urban storm drain systems, Wilmington Drain and Dominguez Channel, all enter into the greater Los Angeles/Long Beach Harbor, which is isolated from the coastal water by an extended breakwater. A smaller urban watershed associated with the Ballona Creek flashed so fast, with high enough plume dilution and dispersion that the elevated FIB area in the Santa Monica Bay was minimal. In all three cases, the FIB is thought to have originated from natural sources (i.e., non-human) and not sewage. By contrast, ocean color was very different and FIB impact was significantly higher in the Tijuana River system than in other SCB coastal areas.

The applicability of offshore water quality measurements, including satellite remote sensing, is an important issue to water quality in the surf zone off the beach where almost all human-water contact happens. MODIS imagery analyzed in this study had a 1-km spatial resolution, and the optical signal of the ocean zone along the coastline (2 - 3 km) was affected by the “stray light effect” (i.e., the sunlight reflected by land). As such, the satellite ocean color measurements could not be directly attributed to beach water quality. However, satellite imagery provides important information about plume size and direction. In particular, it is evident from satellite imagery that channelized river systems that “shoot” runoff offshore, where FIB rapidly decrease below recreational standards, may be a highly efficient and cost effective management strategy for urban stormflow in southern California and other coastal regions.

In the present study, accurate discrimination between plumes and ocean waters was based on the entire visible spectrum (i.e., eight MODIS wavebands 412 - 748 nm). The optical signatures of plumes are modulated by two constituents contributing to ocean color: suspended sediment and CDOM. High concentrations of suspended sediments dominated by lithogenic silica (Toole and Siegel 2001, Warrick *et al.* 2004b) increase backscattering in the central and, to lesser extent, longer wavelength portions of spectra (Otero and Siegel 2004); CDOM absorbs light at short wavelengths (Del Castillo 2005). As a result, the differences between nLw in plume and ocean are most evident for the 531 - 551 nm wavelengths; consequently, these wavelengths proved to be the most informative for MODIS plume detection (at least in this region). The previous studies of freshwater plumes in the SCB were based on

SeaWiFS nLw of 555 nm wavelength (Nezlin and DiGiacomo 2005, Nezlin *et al.* 2005).

The results of this study show that in remotely-sensed plume detection, the chance to classify “ocean” as “plume”, is higher than the chance to classify “plume” as “ocean”; commission errors exceeded omission errors for plumes determined both in terms of salinity and FIB exceedances. However, the accuracy of plume classification in terms of salinity is not directly transferable to FIB counts (i.e., water quality). In the SCB, concentrations of total coliforms, fecal coliforms, and *Enterococcus* sp. in plume waters are typically higher in low salinity waters than in ambient ocean waters (Bay *et al.* 2003, Nezlin *et al.* 2007). However, in this study, the stations for which FIB counts exceeded the California State Water Board standard were often located beyond the plume limits. Low correlation between salinity and bacterial contamination was not surprising because bacteria have a high mortality rate in sunlight (Davies and Evison 1991, Davies-Colley *et al.* 1994, Sinton *et al.* 2002, Noble *et al.* 2004), which can significantly impact FIB counts, while salinity is primarily impacted by mixing alone. Furthermore, the distribution of bacteria concentration is typically quite patchy (e.g., Boehm and Weisberg 2005, Rosenfeld *et al.* 2006). In terms of human health risk, the commission error for ocean water (the chance that areas classified as non-plume (~non-contaminated) waters exceed the FIB contamination standards is an important assessment factor. In the present study, the commission error for “ocean” was as low as 13%, much lower than the commission error for “plume” (78%). This means that of the two types of errors: erroneous plume detection resulting in unjustified beach closures and undetected pathogen-laden plumes resulting in human health risk; the first error type appears to be more probable for remotely-sensed plume monitoring and assessments.

Horizontal advection of plume waters and potential spatial inaccuracy of the MODIS-Aqua satellite imagery (pixel size 1 km) were not significant sources of plume detection errors. This study hypothesized that if spatial inaccuracy was a significant factor, the accuracy of plume detection would increase after smoothing the satellite image by increasing the areas from which classified pixels were selected. For the present study, statistical accuracy was highest when the circular area around stations was minimized ( $R = 1.5$  km), in approximation

to a 3x3-pixel box and smaller than the 5x5-pixel box recommended by Bailey and Werdell (2006) for spatially homogeneous ocean waters. Higher accuracy at smaller pixel box size may result from spatial heterogeneity typical of the coastal ocean. Due to the limited number of stations in this study, all satellite and ship-based data collected on the same day were compared and analysis was not limited to a shorter time window, such as the 6-hour ( $\pm 3$  hours) window recommended by Bailey and Werdell (2006). In other studies focused on the calibration and validation of remotely-sensed data, the observations were considered a match (i.e., coming from a unique station) when all measurements were made within a 12-hour window and within 0.05 degrees (5.6 km at the equator) in both latitude and longitude (Maritorena *et al.* 2006).

The combined NIR-SWIR atmospheric correction algorithm (Wang and Shi 2007) was shown to be the best choice for detection of stormwater plumes in the SCB. Coastal waters (Case 2) are “optically complex” (Morel and Prieur 1977), requiring more sophisticated approaches to atmospheric correction of satellite imagery than open ocean waters (Siegel *et al.* 2000). The main difficulty is that the “black pixel assumption” (i.e., the assumption that water-leaving radiance in NIR is negligible) is true for clean oligotrophic ocean waters, but typically does not work in coastal areas where significant NIR backscattering results from high concentrations of phytoplankton and suspended sediments. In the open ocean, aerosol radiative properties can be determined from NIR remotely-sensed reflectances, which contain a signal from the atmosphere (Gordon and Wang 1994, Gordon 1997). In turbid coastal waters, however, ocean color retrieval is imperfect, with significant errors in derived products often resulting from ocean contributions at the NIR bands (Wang 2007, Wang *et al.* 2007). Using MODIS SWIR instead of NIR wavelengths for atmospheric correction is a promising method (Wang and Shi 2005, 2006, Wang 2007, Wang *et al.* 2007) because in the SWIR the ocean is generally black, even in coastal regions, due to much stronger water absorption (Hale and Querry 1973). By contrast, in non-turbid waters, the NIR method is preferable because the MODIS NIR bands have much better sensor SNR characteristics than the SWIR bands. The combined NIR-SWIR atmospheric correction method based on turbid water detection suggested by Shi and Wang (2007) has been shown to be a good choice for

processing of MODIS-Aqua imagery in coastal waters (Wang and Shi 2007). This capability needs to be incorporated into ocean color processing on a routine, ideally operational, basis to support this and other important coastal management applications.

Overall system improvements in the ability to observe ocean color from satellites, especially increases in spatial, temporal and spectral resolution, will greatly enhance investigators’ ability to use these observations as a tool for studying regional coastal processes and features such as stormwater runoff plumes, as well as harmful algal blooms (Schnitzer *et al.* 2007). Satellite data, even qualitative data (e.g., “plume” and “ocean” classification), provide critical synoptic information (e.g., plume size and location) for coastal managers and decision makers. This information cannot be obtained from ship-based sampling alone, and its use needs to be promoted and facilitated wherever and whenever possible. Along these lines, this study, and its companion papers detailing findings from the Bight '03 Regional Water Quality Program (Ahn *et al.* 2005, Nezlin *et al.* 2007, Warrick *et al.* 2007), provide an important step in incorporating ocean color satellite data into the water quality decision-support systems used by southern California coastal managers.

## LITERATURE CITED

- Ahn, J.H., S.B. Grant, C.Q. Surbeck, P.M. DiGiacomo, N.P. Nezlin and S. Jiang. 2005. Coastal water quality impact of stormwater runoff from an urban watershed in southern California. *Environmental Science & Technology* 39:5940-5953.
- Bailey, S.W. and P.J. Werdell. 2006. A multi-sensor approach for the on-orbit validation of ocean color satellite data products. *Remote Sensing of Environment* 102:12-23.
- Bay, S., B.H. Jones, K. Schiff and L. Washburn. 2003. Water quality impacts of stormwater discharges to Santa Monica Bay. *Marine Environmental Research* 56:205-223.
- Boehm, A.B. and S.B. Weisberg. 2005. Tidal forcing of Enterococci at marine recreational beaches at fortnightly and semidiurnal frequencies. *Environmental Science & Technology* 39:5575-5583.
- Bray, N.A., A. Keyes and W.M.L. Morawitz. 1999. The California Current System in the Southern California Bight and the Santa Barbara Channel.

- Journal of Geophysical Research-Oceans* 104:7695-7714.
- Congalton, R.G. and K. Green. 1999. Assessing the Accuracy of Remotely Sensed Data: Principles and Practices. Lewis Publishers. Boca Raton, FL.
- Curtin, T.B. and R.V. Legeckis. 1986. Physical observations in the plume region of the Amazon River during peak discharge. I. Surface variability. *Continental Shelf Research* 6:31-51.
- D'Sa, E.J. and R.L. Miller. 2003. Bio-optical properties in waters influenced by the Mississippi River during low flow conditions. *Remote Sensing of Environment* 84:538-549.
- Dailey, M.D., J.W. Anderson, D.J. Reish and D.S. Gorsline. 1993. The Southern California Bight: Background and setting. pp. 1-18 in: M. D. Dailey , D. J. Reish and J. W. Anderson (eds.), Ecology of the Southern California Bight. University of California Press. Berkeley, CA.
- Davies-Colley, R.J., R.G. Bell and A.M. Donnison. 1994. Sunlight inactivation of Enterococci and fecal coliforms in sewage effluent diluted in seawater. *Applied and Environmental Microbiology* 60:2049-2058.
- Davies, C.M. and L.M. Evison. 1991. Sunlight and the survival of enteric bacteria in natural waters. *Journal of Applied Microbiology* 70:265-274.
- Del Castillo, C.E. 2005. Remote sensing of organic matter in coastal waters. pp. 157-180 in: R.L. Miller, C.E. Del Castillo and B.A. McKee (eds.), Remote Sensing of Coastal Aquatic Environments. Technologies, Techniques and Applications. Springer. Dordrecht, Netherlands.
- Del Vecchio, R. and A. Subramaniam. 2004. Influence of the Amazon River on the surface optical properties of the western tropical North Atlantic Ocean. *Journal of Geophysical Research-Oceans* 109:C11001.
- DelCastillo, C.E., P.G. Coble, R.N. Conmy, F.E. Muller-Karger, L. Vanderbloemen and G.A. Vargo. 2001. Multispectral in situ measurements of organic matter and chlorophyll fluorescence in seawater: Documenting the intrusion of the Mississippi River plume in the West Florida Shelf. *Limnology and Oceanography* 46:1836-1843.
- Esaias, W.E., M.R. Abbott, I. Barton, O.B. Brown, J.W. Campbell, K.L. Carder, D.K. Clark, R.H. Evans, F.E. Hoge, H.R. Gordon, W.M. Balch, R.M. Leteller and P.J. Minnett. 1998. An overview of MODIS capabilities for ocean science observations. *IEEE Transactions on Geoscience and Remote Sensing* 36:1250-1265.
- Estournel, C., V. Kondrachoff, P. Marsaleix and R. Vehil. 1997. The plume of the Rhone: Numerical simulation and remote sensing. *Continental Shelf Research* 17:899-924.
- Fiedler, P.C. and R.M. Laurs. 1990. Variability of the Columbia River plume observed in visible and infrared satellite imagery. *International Journal of Remote Sensing* 11:999-1010.
- Froidefond, J.-M., A.-M. Jegou, J. Hermida, P. Lazure and P. Castaing. 1998. Variability of the Gironde turbid plume by remote sensing. Effects of climatic factors. *Oceanologica Acta* 21:191-207.
- Gordon, H.R. 1997. Atmospheric correction of ocean color imagery in the Earth Observing System era. *Journal of Geophysical Research-Atmospheres* 102:17081-17106.
- Gordon, H.R. and M. Wang. 1994. Retrieval of water-leaving radiance and aerosol optical thickness over the oceans with SeaWiFS: a preliminary algorithm. *Applied Optics* 33:443-452.
- Hale, G.M. and M.R. Querry. 1973. Optical constants of water in the 200-nm to 200-micrometer wavelength region. *Applied Optics* 12:555-563.
- Harms, S. and C.D. Winant. 1998. Characteristic patterns of the circulation in the Santa Barbara Channel. *Journal of Geophysical Research-Oceans* 103:3041-3065.
- Hickey, B.M. 1993. Physical oceanography. pp. 19-70 in: M.D. Dailey, D.J. Reish and J.W. Anderson (eds.), Ecology of the Southern California Bight. University of California Press. Berkeley, CA.
- Lillesand, T.M. and R.W. Kiefer. 2000. Remote Sensing and Image Interpretation (4th edition). John Wiley & Sons. New York, NY.
- Lira, J., A. Morales and F. Zamora. 1997. Study of sediment distribution in the area of the Panuco River plume by means of remote sensing. *International Journal of Remote Sensing* 18:171-182.

- Lynn, R.J., S.J. Bograd, T.K. Chereskin and A. Huyer. 2003. Seasonal renewal of the California Current: The spring transition off California. *Journal of Geophysical Research-Oceans* 108:3279.
- Maritorena, S., Z. Lee, K. Du, H. Loisel, R. Doerffer, C.S. Roesler, P.E. Lyon, A. Tanaka, M. Babin and O.V. Kopelevich. 2006. Synthetic and in situ data sets for algorithm testing. pp. 13-18 in: Z. Lee (ed.), *Remote Sensing of Inherent Optical Properties: Fundamental, Tests of Algorithms and Applications*, Vol. 5. IOCCG. Nova Scotia, Canada.
- Mertes, L.A.K., M.O. Smith and J.B. Adams. 1993. Estimating suspended sediment concentrations in surface waters of the Amazon River wetlands from Landsat images. *Remote Sensing of Environment* 43:281-301.
- Mertes, L.A.K. and J.A. Warrick. 2001. Measuring flood output from 110 coastal watersheds in California with field measurements and SeaWiFS. *Geology* 29:659-662.
- Miller, R.L. and B.A. McKee. 2004. Using MODIS Terra 250 m imagery to map concentrations of total suspended matter in coastal waters. *Remote Sensing of Environment* 93:259-266.
- Miller, R.L., B.A. McKee and E.J. D'Sa. 2005. Monitoring bottom sediment resuspension and suspended sediments in shallow coastal waters. pp. 259-276 in: R.L. Miller, C.E. Del Castillo and B.A. McKee (eds.), *Remote Sensing of Coastal Aquatic Environments*. Springer. Dordrecht, Netherlands.
- Miller, S.N., W.G. Kepner, M.H. Mehaffey, M. Hernandez, R.C. Miller, D.C. Goodrich, K.K. Devonald, D.T. Heggem and W.P. Miller. 2002. Integrating landscape assessment and hydrologic modeling for land cover change analysis. *Journal of the American Water Resources Association* 38:915-929.
- Monahan, E.C. and M.J. Pybus. 1978. Colour, UV absorbance and salinity of the surface waters off the west coast of Ireland. *Nature* 274:782-784.
- Morel, A. and L. Prieur. 1977. Analysis of variations in ocean color. *Limnology and Oceanography* 22:709-722.
- Muller-Karger, F.E., C.R. McClain, T.R. Fisher, W.E. Esaias and R. Varela. 1989. Pigment distribution in the Caribbean Sea: Observations from space. *Progress in Oceanography* 23:23-64.
- Nezlin, N.P. and P.M. DiGiacomo. 2005. Satellite ocean color observations of stormwater runoff plumes along the San Pedro Shelf (southern California) during 1997 to 2003. *Continental Shelf Research* 25:1692-1711.
- Nezlin, N.P., P.M. DiGiacomo, E.D. Stein and D. Ackerman. 2005. Stormwater runoff plumes observed by SeaWiFS radiometer in the Southern California Bight. *Remote Sensing of Environment* 98:494-510.
- Nezlin, N.P., P.M. DiGiacomo, S.B. Weisberg, D.W. Diehl, J.A. Warrick, M.J. Mengel, B.H. Jones, K.M. Reifel, S.C. Johnson, J.C. Ohlmann, L. Washburn and E.J. Terrill. 2007. Southern California Bight 2003 Monitoring Program: V. Water Quality. Southern California Coastal Water Research Project. Costa Mesa, CA.
- Noble, R.T., I.M. Lee and K.C. Schiff. 2004. Inactivation of indicator bacteria from various sources of fecal contamination in seawater and freshwater. *Journal of Applied Microbiology* 96:464-472.
- Noble, R.T., S.B. Weisberg, M.K. Leecaster, C.D. McGee, J.H. Dorsey, P. Vainik and V. Orozco-Borbon. 2003. Storm effects on regional beach water quality along the southern California shoreline. *Journal of Water and Health* 1:23-31.
- Opsahl, S. and R. Benner. 1998. Photochemical reactivity of dissolved lignin in river and ocean waters. *Limnology and Oceanography* 43:1297-1304.
- Otero, M.P. and D.A. Siegel. 2004. Spatial and temporal characteristics of sediment plumes and phytoplankton blooms in the Santa Barbara Channel. *Deep-Sea Research II* 51:1129-1149.
- Ouillon, S., P. Forget, J.-M. Froidefond and J.-J. Naudin. 1997. Estimating suspended matter concentrations from SPOT data and from field measurements in the Rhone River plume. *Marine Technology Society Journal* 31:15-20.
- Richards, J.A. 1999. *Remote Sensing Digital Image Analysis*. Springer-Verlag. Berlin, Germany.
- Rosenfeld, L.K., C.D. McGee, G.L. Robertson, M.A. Noble and B.H. Jones. 2006. Temporal and spatial variability of fecal indicator bacteria in the surf zone

- off Huntington Beach, CA. *Marine Environmental Research* 61:471-493.
- Schiff, K.C., M.J. Allen, E.Y. Zeng and S.M. Bay. 2000. Southern California. *Marine Pollution Bulletin* 41:76-93.
- Schnetzer, A., P.E. Miller, R.A. Schaffner, B.A. Stauffer, B.H. Jones, S.B. Weisberg, P.M. DiGiacomo, W.M. Berelson and D.A. Caron. 2007. Blooms of Pseudo-nitzschia and domoic acid in the San Pedro Channel and Los Angeles Harbor areas of the Southern California Bight, 2003-2004. *Harmful Algae* 6:372-387.
- Shi, W. and M. Wang. 2007. Detection of turbid waters and absorbing aerosols for the MODIS ocean color data processing. *Remote Sensing of Environment* 110:149-161.
- Siddorn, J.R., D.G. Bowers and A.M. Hogue. 2001. Detecting the Zambezi River plume using observed optical properties. *Marine Pollution Bulletin* 42:942-950.
- Siegel, D.A., M. Wang, S. Maritorena and W. Robinson. 2000. Atmospheric correction of satellite ocean color imagery: The black pixel assumption. *Applied Optics* 39:3582-3591.
- Siegel, H., M. Gerth and A. Mutzke. 1999. Dynamics of the Oder River plume in the Southern Baltic Sea: satellite data and numerical modeling. *Continental Shelf Research* 19:1143-1159.
- Sinton, L.W., C.H. Hall, P.A. Lynch and R.J. Davies-Colley. 2002. Sunlight inactivation of fecal indicator bacteria and bacteriophages from waste stabilization pond effluent in fresh and saline waters. *Applied and Environmental Microbiology* 68:1122-1131.
- State Water Resources Control Board. 2005. California Ocean Plan. State Water Resources Control Board. Sacramento, CA.
- Strub, P.T., J.S. Allen, A. Huyer and R.L. Smith. 1987. Large-scale structure of the spring transition in the coastal ocean off western North America. *Journal of Geophysical Research-Oceans* 92:1527-1544.
- Strub, P.T. and C. James. 1988. Atmospheric conditions during the spring and fall transition in the coastal ocean off western United States. *Journal of Geophysical Research-Oceans* 93:15561-15584.
- Toole, D.A. and D.A. Siegel. 2001. Modes and mechanisms of ocean color variability in the Santa Barbara Channel. *Journal of Geophysical Research-Oceans* 106:26985-27000.
- Vasilkov, A.P., V.I. Burenkov and K.G. Ruddick. 1999. The spectral reflectance and transparency of river plume waters. *International Journal of Remote Sensing* 20:2497-2508.
- Vodacek, A., N.V. Blough, M.D. DeGrandpre, E.T. Peltzer and R.K. Nelson. 1997. Seasonal variation of CDOM and DOC in the Middle Atlantic Bight: Terrestrial inputs and photooxidation. *Limnology and Oceanography* 42:674-686.
- Walker, N.D. 1996. Satellite assessment of Mississippi river plume variability: Causes and predictability. *Remote Sensing of Environment* 58:21-35.
- Wang, M. 2007. Remote sensing of the ocean contributions from ultraviolet to near-infrared using the shortwave infrared bands: Simulations. *Applied Optics* 46:1535-1547.
- Wang, M. and W. Shi. 2005. Estimation of ocean contribution at the MODIS near-infrared wavelengths along the east coast of the US: Two case studies. *Geophysical Research Letters* 32:L13606.
- Wang, M. and W. Shi. 2006. Cloud masking for ocean color data processing in the coastal regions. *IEEE Transactions on Geoscience and Remote Sensing* 44:3196-3205.
- Wang, M. and W. Shi. 2007. The NIR-SWIR combined atmospheric correction approach for MODIS ocean color data processing. *Optics Express* 15:15722-15733.
- Wang, M., J. Tang and W. Shi. 2007. MODIS-derived ocean color products along the China east coastal region. *Geophysical Research Letters* 34:L06611.
- Warrick, J.A., P.M. DiGiacomo, S.B. Weisberg, N.P. Nezlin, M.J. Mengel, B.H. Jones, J.C. Ohlmann, L. Washburn, E.J. Terrill and K.L. Farnsworth. 2007. River plume patterns and dynamics within the Southern California Bight. *Continental Shelf Research* 27:2427-2448.
- Warrick, J.A. and D.A. Fong. 2004. Dispersal scaling from the world's rivers. *Geophysical Research Letters* 31:L04301.

Warrick, J.A., L.A.K. Mertes, D.A. Siegel and C. MacKenzie. 2004a. Estimating suspended sediment concentrations in turbid coastal waters of the Santa Barbara Channel with SeaWiFS. *International Journal of Remote Sensing* 25:1995-2002.

Warrick, J.A., L.A.K. Mertes, L. Washburn and D.A. Siegel. 2004b. A conceptual model for river water and sediment dispersal in the Santa Barbara Channel, California. *Continental Shelf Research* 24:2029-2043.

Warrick, J.A., L.A.K. Mertes, L. Washburn and D.A. Siegel. 2004c. Dispersal forcing of southern California river plumes, based on field and remote sensing observations. *Geo-Marine Letters* 24:46-52.

Warrick, J.A. and J.D. Milliman. 2003. Hyperpycnal sediment discharge from semiarid southern California rivers: Implications for coastal sediment budgets. *Geology* 31:781-784.

Washburn, L., B.H. Jones, A.W. Bratkovich, T.D. Dickey and M.-S. Chen. 1992. Mixing, dispersion, and resuspension in vicinity of ocean wastewater plume. *Journal of Hydraulic Engineering-ASCE* 118:38-58.

## **ACKNOWLEDGEMENTS**

The authors would like to thank Wei Shi for help in processing MODIS data and the National Aeronautics and Space Administration (NASA) Goddard Space Flight Center (GSFC) for the production and distribution of the MODIS data and images. MODIS data were acquired as part of the NASA's Earth Science Enterprise and were processed by the MODIS Adaptive Processing System (MODAPS), archived and distributed by the Goddard Distributed Active Archive Center (DAAC). The authors thank all participants of the Bight'03 Regional Water Quality Program. Critical comments of Alex Steele, Ivan Valiela and two anonymous reviewers helped to improve the paper significantly. This work was partly supported by a NASA Oceans & Ice Research Award (NRA-04-OES-02) from the NASA Ocean Biology and Biogeochemistry Program (Dr. Paula Bontempi, Program Scientist). The contents of this article are solely the opinions of the authors and do not constitute a statement of policy, decision, or position on behalf of the United States Geological Survey (USGS), the National Oceanic and Atmospheric Administration (NOAA) or the US Government.